PCCP

Accepted Manuscript

ROYAL SOCIETY OF CHEMISTRY

www.rsc.org/pccp

ARTICLE TYPE www. rsc.org/xxxxxx | XXXXXXXX

Optical Properties of Prodigiosin and Obatoclax. Action Spectroscopy and Theoretical Calculations.

Evangeline Drink,[a], Philippe Dugourd[a], Elise Dumont[b], Nils Aronssohn[b], Rodolphe Antoine[a,*], Claire Loison[a,*]

Received Xth XXXXXXXXXX 20XX, Accepted Xth XXXXXXXXX 20XX
First published on the web Xth XXXXXXXXXX 200X
DOI: 10.1039/b000000x

Prodiginine molecules (prodigiosin and obatoclax) are well-known pH-chromic dyes with promising anti-tumor activities. They present multiple tautomeric and rotameric forms. The protonation state and the structure of such flexible ligands in interaction with a protein is crucial to understand and to model the protein biological activities. The determination of the protonation state via the UV/vis absorption is possible if the ligand spectra of the neutral and protonated states are sufficiently different, and also if we can eliminate other factors potentially impacting the spectrum. Measuring absorption spectra of the ligand in solution, varying solvents and pH values, we have determined that the optical properties of prodigiosin and obatoclax depend on the protonation state and not on the solvent permittivity constant. In parallel, action spectroscopy (using tunable lasers coupled to ion traps) in the gas phase of protonated and sodiated prodigiosin and obatoclax molecules has been performed to evaluate the sensitivity of the charge and conformational state on their optical properties free of solvent. The spectra are interpreted using computational simulations of molecular structures and electronic excitations. The excitation energies are only slightly sensitive to various isomerizations, and may be used to distinguish between protonated and deprotonated states, even in the presence of a sodium counter-ion.

1 Introduction

Prodiginines are tripyrrole compounds produced as secondary metabolites by several terrestrial and marine microorganisms [1–6]. Their intense red color has raised attention a thousand years ago [7], but their very promising antitumor, immunosuppressant, and antimalarial properties have been discovered much more recently (for a review see Ref. 8).

The natural prodigiosin (PG, see Fig. 1, a and b) is able to induce apoptosis in many different human cancer cell lines with little effect on non-malignant cells [9,10]. A synthetic prodiginin, obatoclax, (OBX, see Fig. 1c,d) is promising as a drug against a variety of hematological malignancies [11–15] and solid tumors [16]. The mechanisms of prodiginins antitumoral actions are still debated ; one may cite their interactions with anti-apoptotic B-cell lymphocyte/leukemia-2 (Bcl-2) proteins [10], their efficiency as ions receptors and transporters within the cell [17–20], and the copper-mediated cleavage of double-stranded DNA [21,22]. In contrast to the promising results on cell lines and on mice models, its disappointing inefficiency as anti-tumoral agent in clinical trials raises many questions [10,23–26].

By understanding the molecular mechanism of prodiginins' biochemistry and mechanism of action, their potential for the treatment of malignancies may be further clarified. In particular, prodiginins may exist in a number of different isomers and protonation states, which may have different biological impact. Depending on their environment, different isomers or charge states may be favored. For example, the crystal structure and solution formation constant of the HCl-complex of PG and some derivatives have been determined [19,27,28]. In these crystals, the protonated form of prodigiosin (PG-H^+) is observed in a conformer where the chloride counter-ion is in the center of the three protonated nitrogens forming a tweezer, and noted β (see Fig. 1a). But Garcìa-Valverde et al. have calculated that in polar solution, PG-H^+ should adopt a different conformation noted γ, where the three nitrogens do not form a tweezer (see Fig. 1b) [29]. Rizzo et al. also have succeeded to separate two rotamers of a derivative of PG-H^+ [30], and showed that they may have similar absorption spectra, but different pKa. Therefore, the pKa measured spectrophotometric titrations (7.2 for PG-H^+/PG and 7.9 for OBX-H^+/OBX) are macroscopic equilibrium acidity constants emerging from several concomitant titrations of different conformers in equilibrium.

In a biological context, when prodiginins interact as a ligand, for instance with Bcl-2 proteins, the protonation state and conformation of the ligand may depend on the position of the ligand and on its interactions with the protein [31]. To

[a] *Institut Lumière Matière, UMR5306 Université Lyon 1-CNRS, Université de Lyon 69622 Villeurbanne cedex, France.* [b] *Laboratoire de Chimie, UMR5182, Ecole Normale Supérieure de Lyon, 69364 Lyon cedex 07, France.*
∗ *Corresponding authors. E-mail addresses: rodolphe.antoine@univ-lyon1.fr; claire.loison@univ-lyon1.fr*

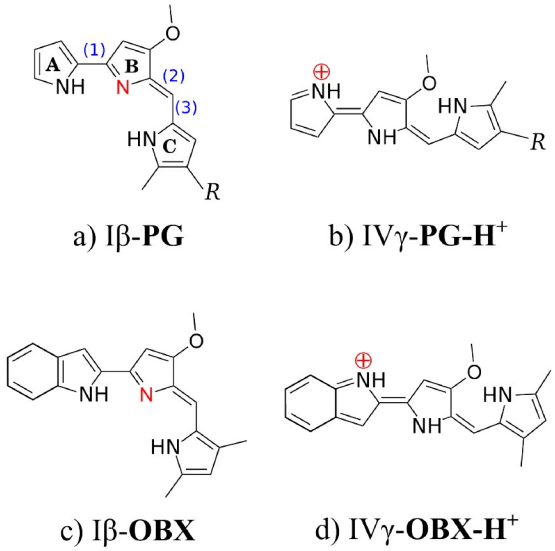

Fig. 1 Structures of prodigiosin (PG) in its neutral (a) and protonated (b) forms; structures of obatoclax (OBX) in its neutral (c) and protonated (d) forms. In natural prodigiosin, the residue R is C_5H_{11}; in our theoretical model, it is C_2H_5. Among the possible rotamers and tautomers obtained by rotations around the bonds noted (1), (2), and (3) and by various protonation states of the nitrogen atoms of cycles A, B and C, the isomers $I\beta$ and $IV\gamma$ shown here are the ones with the lowest energies (ωB97X-D/6-311++G(d,p) level of calculation). Color online.

understand the biological action mechanism of prodiginins in interaction with other biomolecules, one needs to investigate which isomers are present, and which are active. Protein X-ray crystallography represents an experimental method heavily applied in all stages of drug discovery. As an alternative, Nuclear Magnetic Resonance also provides information on ligand/protein complexes at the atomic scale[32,33]. These techniques would probably enable differentiation between β and γ conformers, but they might not have sufficient resolution to draw conclusions about the protonation state in a complex environment. Prediction of protonation state in biomimetic environments using theoretical modeling also remains a difficult task[34,35].

Tunable lasers in the UV-visible range coupled with mass spectrometry permit to do energy-resolved photodissociation (PD) experiments. This tecFhnique, also noted as action spectroscopy, monitors the photodissociation or photodetachment yield as a function of the laser wavelength and is directly related to optical absorption[36]. Action spectroscopy on trapped model bio-chromophores was pioneered by Nielsen, Andersen and colleagues, using electrostatic storage devices (ELISA)[37]. This approach was successfully explored on various protein model chromophores[38–42]. Our group used electron photodetachment to report the first electronic excitation spectra of isolated biomolecular ions[43,44], and pushed forward the limit of spectroscopy on large isolated biomolecular ions in the visible[45], UV[46] and even VUV range[47,48].

Therefore, PD spectroscopy would be an efficient approach to investigate the structure of prodiginins in complex biological environments. The determination of the protonation state via the UV/vis absorption is possible only if the ligand spectra of the neutral and protonated states are sufficiently different, and also if we can eliminate other factors potentially impacting the spectrum. Before investigating prodiginins in biomimetic environments, we first need to characterize them in model environments, assess their solvatochromic properties, and investigate the link between their structural and optical properties.

In this paper, we report a joint experimental and theoretical investigation of the optical properties of isolated prodiginins. We focus on the impact of protonation on their structural and optical properties. Moreover, we have studied the impact of the interaction with a cation on the absorption spectrum, the first stage towards more complex environments. Both sodium and potassium cations would be relevant in a biological context, but the ion signal observed in mass spectra is significantly higher for sodium adducts than for potassium adduct, so that this work focuses on sodium adducts. We show that the natural ligand and dye prodigiosin (PG), and its derivative obatoclax (OBX), are good candidates as optical probes of their protonation state. In parallel, theoretical calculations have been used to interpret and model the effects of protonation and structural modifications on the optical properties of PG and OBX.

2 Materials and Methods

2.1 Materials.

Prodigiosin was bought from AdipoGen (Liestal, Switzerland) and obatoclax Mesylate (97.95% purity) was purchased from Selleckchem.com (Houston, TX). Dimethyl Sulfoxide (DMSO) was purchased from Sigma (St. Louis, MO) and 1 N HCL solution in water was bought from Sigma-Aldrich (Steinhelm, Germany). Ethanediol (Ethylene Glycol) was purchased from Acros Organics (New Jersey, USA). Fisher Scientific UK (Loughborough, UK) was the supplier of Ethanol, absolute (analytical reagent grade) and Methanol (HPLC grade).

2.2 UV/vis absorption in solution.

UV-Vis spectra were recorded applying an AvaSpec-2048 Fiber optic spectrometer, an AvaLight-DH-S deuterium-halogen light source, and a UV-VIS cuvette by Avantes. All solvents were of spectrophotometric grade. In addition, we have explored the fluorescence emissions properties of the two molecules

and could not measure any fluorescence signal in the visible range, in agreement with the results reported by Dimitrov et al. on prodigiosin[49]. Han et al. reported that PG emits weak luminescence in Tris-HCl buffer (pH 6.8) at room temperature, with a fluorescence maximum appearing at 554 nm, when excited at 520 nm[50]. It was nevertheless reported that prodiginins may fluoresce when they interact with other molecules[49,50]. The weakness of fluorescence indicates the existence of radiationless deactivation channels. The increase of fluorescence intensity when the aromatic cycle interact with other molecules[49,50] might indicate that these radiationless deactivation are linked to rotamer interconversions.

2.3 Mass Spectrometry and visible Photodissociation.

Positive ion electrospray was used with solution concentration of 20 μM prodigiosin and 20 μM obatoclax in 1:1 ethanol/water. 10 μL of 1N HCl was added to solutions to protonate prodigiosin and obatoclax. 10 μL of 1N NaCl was added to solutions to sodiate prodigiosin and obatoclax. Two modes of fragmentation were used: collision-induced dissociation (CID) which consists in fragmenting the trapped ions by collisions with He atoms in the ion trap and photodissociation (PD), which consists in fragmenting the trapped ions by irradiating them with photons. CID was accomplished using helium gas at a normalized collision energy of 35% for 30 ms. The activation q value was set to 0.200 for CID and for PD. The isolation width for selecting the ion precursors (both for PD and CID) was 3 Da. A total of 50 microscans were averaged to produce a spectrum. The laser is a 10 Hz-nanosecond frequency-doubled tunable Panther^{TM} EX OPO laser pumped by a Powerlite^{TM} II Nd:YAG laser (both from Continuum, Santa Clara, CA, USA). The laser beam passes through two diaphragms (2 mm diameter) and lenses after which it is injected on the axis of the linear trap through a quartz window fitted on the rear of the LTQ Velos chamber[51]. An electromechanical shutter, electronically synchronized with the mass spectrometer, was placed along the laser beam and allowed to inject the laser light according to a given time sequence. To perform laser irradiation, the ion cloud was irradiated for 1000 ms (10 laser shots). We added in the ion trap RF sequence an MS^n step with an activation amplitude of 0%, during which the shutter located on the laser beam is opened. The different steps of ion selection and excitation are successively carried out in the high pressure cell. Final product ions are then transferred and mass analyzed in the low pressure cell. The photofragmentation yield is defined as $\sigma = \ln\left(\left(I_p + \Sigma_f\right)\right) / \left(I_p \Phi\right)$ where I_p and Σ_f are the intensity of the precursor ion signals and sum of photofragments and Φ is the laser fluence. Three action spectra are averaged together for the reported spectra.

2.4 Theoretical Calculations

In this study, we have systematically made the common quantum mechanical approximation of replacing Progidiosin alkyl chain (C_5H_{11}) by an ethyl group (C_2H_5). Tossel et al. have shown that this approximation does not change qualitatively their results on the conformers stability and electronic excitation energies[52]. All calculations have been performed with the version D.01 of the Gaussian 09 program package[53], applying a tight self-consistent field convergence criterion (10^{-9} to 10^{-10} a.u.) and a strict optimization threshold (10^{-5} a.u. on average forces). We have optimized both the ground and excited state geometries and determined their vibrational patterns using density functional theory (DFT) and its time-dependent derivation (TDDFT), respectively. The same integration grid, namely the ultrafine grid, was used. We calculate vibrational spectra at the harmonic level, and the absence of imaginary frequencies confirms that we are at a local minimum. We have used the 6-311++G(d,p) atomic basis set throughout, which is expected to produce converged data for low-lying excited states in organic molecules. We compared the stability of different isomers using the total electronic energy with zero-point correction (ZPC). Discussions about the most appropriate exchange-correlation functionals are developed in greater detail in Refs. 54–57. ωB97X-D[58] emerged as a functional able to reproduce, in a balanced way, both local and inter-base charge-transfer excited states, and also valuable in simulation of the impact of the environment on electronic excitation[54,59]. Therefore, we have used this functional for geometry optimization of ground and excited states. Nevertheless, to get some insight into the effect of functional on the vertical excitation energies of prodiginins, we compared the vertical excitation energies obtained by B3LYP[60], τ-HCTH[61], CAM-B3LYP[62], PBE0[63], M11[64] and ωB97X-D[58], at the fixed geometry obtained previously by ωB97X-D/6-311++G(d,p) optimizations. The global hybrid B3LYP Becke:1993tm is very often used in the quantum chemistry community. One popular meta-GGA is used here : τ-HCTH. The global hybrids PBE0 and Truhlars global hybrid M11 have proven to give very reasonable results for organic chromophores[55], and are adapted to describe charge-transfer electronic excitations[65]. Long-range correction is proposed with CAM-B3LYP and ωB97X-D. The ωB97X-D also includes an empirical correction to take into account dispersion effects.

Vibrationally resolved spectra within the harmonic approximation were computed using the FC module of Gaussian 09[66,67]. Excited state geometry and vibrations were obtained with functional ωB97X-D, which is usually relatively accurate for such studies, especially where a twisted/planar intramolecular charged-transfer equilibrium is possible[54]. Our calculations, based on the Franck-Condon formalism, are performed for molecules at 0K. A maximal number of 30 overtones for each mode and

30 combination bands on each pair of modes were included in the calculation. The maximum number of integrals to be computed for each class was set to 10^{10}. The convergence of the FC factor was 0.94 for Iβ-PG and 0.90 for Iβ-PG-H$^+$. The reported spectra were simulated using a convoluting Gaussian function presenting a half width at half maximum (HWHM) that was adjusted to approaches spectra similar to experiment ones (typical value: 0.09 eV $\simeq$ 750 cm^{-1}). To match the maxima of the absorption band with the experimental action spectra, on Fig 3, the transition energies obtained using ωB97X-D have been shifted by -0.37 eV.

3 Results

3.1 Solvatochromism

Absorption spectra of prodigiosin have been recorded in various alcohol/water mixtures in the past and at different pH values[27,68]. Two peaks are observed in the visible part of the spectrum with maxima at 537 nm and 470 nm (2.31 and 2.64 eV respectively). The lower energy peak dominates at acid pH and the higher energy one at basic pH.

To determine the possible influence of solvation on the optical spectra, we recorded UV-Vis absorption spectra of prodigiosin and obatoclax in pure solvents that have various dielectric constants. The results of the protonated prodigiosin and obatoclax molecules are displayed Figs. **??** and **??** in Electronic Supplementary Information (ESI). Based on these two graphs, when using solvents that have varying dielectric constants within the range of 2 until 47, the absorption wavelengths of either molecule barely shifted, for both the protonated and the neutral molecules. These results show that even with varying the polarity of the solvent (dielectric constant), prodigiosin and obatoclax are not affected by the solvents polarity and are thus not solvatochromic.

3.2 Action Spectroscopy

PG and derivatives have already been studied using mass spectrometry by Chen and co-workers[69], who showed that protonated PG mainly dissociates via the methyl radical loss and consecutive fragment ions, and in a lesser extent by the loss of a methanol molecule. Since 15 Da loss is common to MS/MS spectra of all prodiginines, it was suggested that this corresponds to the loss of the methyl moiety of the methoxy group on the B-ring. In this work, protonated prodigiosin and obatoclax have the same fragmentation pathways with the loss of the methyl radical being more prevalent than the loss of the methanol group. The same fragments are observed either by collision activation (CID) or light absorption (and do not depend on the laser wavelength), while their relative abundance is slightly different (see Figs. **??** and **??** and in ESI). For sodiated prodigiosin, the15 Da loss is the main fragmentation channel along with the loss of C_4H_9 radical. Interestingly, for sodiated obatoclax, in addition to the loss of methanol molecule, bigger neutral losses are observed that might correspond to fragments within rings.

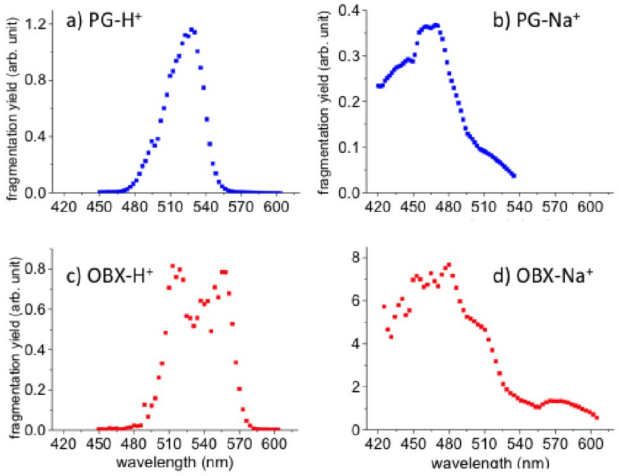

Fig. 2 Experimental gas phase photofragmentation yield of (a-b) protonated and sodiated prodigiosin and (c-d) protonated and sodiated obatoclax.The definition of the yield is given in the Experimental Section. Color online.

Fig. 2 shows the action spectra of protonated and sodiated prodigiosin and obatoclax molecules in the gas phase. The absorption peak in Figure 2a is at 522 nm (2.37 eV). For a comparison, based on the absorption spectra of protonated prodigiosin in the liquid phase (varying between 530-540 nm), the gas phase absorption of prodigiosin is slightly blue shifted (see Fig. **??**). Furthermore, it should be noted that there are two peaks for the protonated obatoclax molecule, one at 519 nm (2.39 eV) and the other at 554 nm (2.23 eV), which are not observed for the protonated obatoclax in the liquid phase (absorption peaks ranging from 544 nm to 550 nm) with only one protonated absorption peak. Concerning sodiated species, spectra are blue-shifted and much broader (in particular for obatoclax) as compared to those of the protonated species. One qualitative difference between prodigiosin and obtatoclax in the action mass spectra is the presence of a double peak for OBX-H$^+$ (see Fig. 2c). The splitting of the band might originate in various phenomena : (1) the presence of several conformers with different excitation energies, (2) the appearance of several excitation levels for a single conformers, (3) or intense vibronic couplings for a single electronic excitation. These are discussed on the basis of our theoretical results in Sect. 3.3.2. Finally, gas phase spectra of sodiated prodiginine

molecules are very similar to the absorption spectra of neutral prodigiosin in the liquid phase (see Fig. **??**). Solvation has only a small impact on the position of the optical spectra.

3.3 Theoretical calculations

3.3.1 Numerous tautomers and rotamers

The conjugated moiety of prodiginin is expected to adopt a rather planar conformation. Three bonds linking the cycles A, B and C (see Fig. 1) permit to imagine $2^3 = 8$ different rotamers of the aromatic core. Moreover, for the neutral form of the prodiginin, only two of the three nitrogen atoms are protonated, which let three different tautomers emerge. Following the notations by Garcìa-Valverde et al.[29] (different from Tossel's one[52]), we distinguish the different rotamers using greek letters (α to θ), and the different tautomers using roman numbers (I, II, III for the neutral form, IV for the protonated form, where the three nitrogens cary a proton). Figs. **??** and **??** in ESI describe the $8 \times 4 = 32$ resulting isomers of prodigiosin (PG) and obatoclax (OBX).

Chen et al.[69], Tossel et al.[52] and Garcìa-Valverde et al.[29] have already discussed the relative stability of prodiginins isomers. We complete their studies by comparing the energies of all the possible isomers of our model of prodigiosin and of obatoclax, in the neutral and protonated forms. The relative total energies are given in Figs. **??** and **??** of ESI.

For neutral prodigiosins, the tautomers of type I are favored, i.e. the protonated nitrogens are on cycle A and C, while the nitrogen on cycle B is deprotonated. The isomer Iβ-PG is the most stable (see Fig. 1a), followed by Iδ-PG, which energy is 11.8 kJ.mol^{-1} higher. The same isomer Iβ was found for a very similar prodiginin by Garcìa-Valverde et al. using solution ^{1}H and ^{13}C NMR experiments and quantum chemical calculations[29]. Even if the subtituants of their model are slightly different from ours, the relative energies of the conformers existing in both models are in very good agreement. One can reasonably consider that at equilibrium, the Iβ population is dominant (at 300K, the thermal energy k_BT equals 2.5 kJ.mol^{-1}). For the protonated species, the two elongated rotamers IVγ-PG-H$^+$ and IVα-PG-H$^+$ have the lowest energy, with IVγ-PG-H$^+$ dominant (its energy+ZPC is lower by 6 kJ.mol^{-1}), see Fig. 1b. For obatoclax, the same rotamer Iβ-OBX is obtained for the neutral form, but for the protonated OBX-H$^+$, the two rotamers IVγ and IVα may be present at room temperature (see Fig. 1b). Noticeably, the formal acido-basic equilibrium Iβ-PG + H$^+$ $\rightleftharpoons$ IVγ-PG-H$^+$ involves rotations around the bonds noted (1) and (2) on Fig. 1, so that other rotamers appear as transition states or reaction intermediates. Garcìa-Valverde et al. have indeed observed the NMR fingerprint of rotamer conversion upon a change of counterion in DMSO solution[29]. For a derivative of PG in solution, Rizzo et al. have also shown that the rotation around the bond noted (2) is rapid for the neutral form, but it is frozen for the protonated form, hindered by the intramolecular H-bond[30].

3.3.2 Excitation Energies Calculations

Given the conformation of most stable isomers of neutral and protonated PG and OBX, one can model their UV-visible absorption spectra by calculating the energies $\Delta E = hc/\lambda$ which the molecule may absorb during an electronic excitation by a photon of wavelength λ. If one neglects the variation of geometry and vibration modes upon the electronic excitation, these excitation energies can be estimated by a time-dependent density functional theory (TDDFT) calculation at the ground state geometry. Table 1 gathers the vertical absorption energies obtained for our model of prodigiosin and obatoclax. Comparisons are made between prodigiosin in the protonated state (the two lowest energy conformers IVγ and IVα, plus IVβ for comparison), in the neutral state (the lowest energy conformer Iβ, plus two conformers for comparison), and in interaction with Na$^+$. We report the vertical excitation energy for the lowest-energy conformers, plus for one or two other conformers for comparison (their relative energy are given in parenthesis). Moreover, comparison is made between different functionals. In most cases, a single electronic excitation was dominant, with an oscillator strength larger than 0.8, and it corresponds to the HOMO-LUMO transition (Highest Occupied Molecular Orbital to Lowest Unoccupied Molecular Orbitals).

3.3.2.1 Protonated and neutral prodigiosin

We first compare the results for lowest energy conformers: the neutral Iβ-PG and the protonated IVγ-PG-H$^+$. The vertical excitation energies depend on the functional, but a global tendency is recognizable : deprotonation increases the excitation energies, by values varying from 0.15 to 0.28 eV depending on the functional. The neutral forms also have lower oscillator strengths, associated to lower absorption intensities. These shifts of wavelengths and intensities are indeed observed for prodigiosin in solution of varying pH. More quantitatively, if one takes the maximum of the experimental absorption spectra of prodigiosin solutions (see Fig. **??**), the excitation energies are shifted from about 2.34 eV for PG-H$^+$ to about 2.70 eV for PG, i.e. a shift of 0.26 eV. Additionally, one can investigate the impact of conformation on the vertical excitation energies. Different isomers of neutral PG have a small spreading of their excitation energies. The dominant isomers are described in Table 1. If one investigates the whole data obtained using ωB97X-D/6-311++G(d,p) (not shown here), seven rotamers of the tautomers of type I of neutral PG (Iα to Iθ, except Iδ) have vertical excitation energies ranging from 3.06 eV to 3.18 eV. The same is true for PG-H$^+$: the eight rotamers of type IV (IVα to IVθ, except IVδ) have vertical excitation energies ranging from 2.78 eV to 2.86 eV (also using ωB97X-

prodigiosin	PG-H^+			PG			PG-Na^+	
Isomer (kJ.mol^{-1})	IVγ (0)	IVα (6)	IVβ(23)	Iβ (0)	Iγ (38)	Iζ (43)	Iζ (0)	Iβ(12)
Functional	Δ**E** f	Δ**E** f	Δ**E** f	Δ**E** f	Δ**E** f	Δ**E** f	Δ**E** f	Δ**E** f
τ-HCTH	**2.53** *0.95*	**2.59** *1.04*	**2.60** *0.80*	**2.71** *0.60*	**2.53** *0.54*	**2.62** *0.52*	**2.56** *0.47*	**2.69** *0.36*
B3LYP	**2.70** *1.18*	**2.75** *1.27*	**2.72** *0.90*	**2.85** *0.77*	**2.79** *0.74*	**2.82** *0.73*	**2.77** *0.56*	**2.98** *0.45*
PBE0	**2.75** *1.23*	**2.80** *1.32*	**2.77** *0.93*	**2.95** *0.80*	**2.86** *0.80*	**2.89** *0.77*	**2.84** *0.60*	**3.07** *0.47*
CAM-B3LYP	**2.82** *1.29*	**2.85** *1.37*	**2.81** *0.97*	**3.08** *0.86*	**3.07** *0.96*	**3.04** *0.87*	**3.04** *0.63*	**3.35** *0.51*
M11	**2.84** *1.28*	**2.86** *1.35*	**2.83** *0.97*	**3.16** *0.88*	**3.18** *1.02*	**3.14** *0.90*	**3.17** *0.64*	**3.48** *0.46*
ωB97X-D	**2.83** *1.30*	**2.86** *1.37*	**2.83** *0.98*	**3.10** *0.97*	**3.10** *0.96*	**3.06** *0.87*	**3.09** *0.65*	**3.38** *0.47*
obatoclax	OBX-H^+			OBX			OBX-Na^+	
Isomer (kJ.mol^{-1})	IVγ (0)	IVα (4)	IVβ(20)	Iβ (0)	Iγ(36)	Iζ(51)	Iγ(0)	Iα(1)
Functional	Δ**E** f	Δ**E** f	Δ**E** f	Δ**E** f	Δ**E** f	Δ**E** f	Δ**E** f	Δ**E** f
τ-HCTH	**2.25** *0.79*		**2.40** *0.75*	**2.56** *0.35*	**2.25** *0.30*	**2.37** *0.31*	**2.35** *0.13*	
	2.46 *0.95*	**2.30** *0.81*	**2.93** *0.27*	**2.65** *0.37*	**2.65** *0.37*	**2.74** *0.29*	**2.58** *0.46*	**2.55** *0.65*
					3.05 *0.17*	**2.97** *0.32*		
B3LYP	**2.25** *0.23*	**2.37** *0.37*	**2.44** *0.36*					
	2.55 *0.93*	**2.60** *0.84*	**2.63** *0.63*	**2.82** *0.91*	**2.70** *0.63*	**2.69** *0.64*	**2.80** *0.80*	**2.82** *1.07*
PBE0	**2.38** *0.41*	**2.49** *0.66*	**2.55** *0.64*		**2.62** *0.68*			
	2.65 *0.83*	**2.70** *0.63*	**2.73** *0.39*	**2.89** *0.95*	**2.71** *0.77*	**2.78** *0.71*	**2.89** *0.95*	**2.89** *1.14*
CAM-B3LYP	**2.70** *1.34*	**2.74** *1.45*	**2.72** *1.09*	**3.02** *0.99*	**2.97** *1.06*	**2.98** *0.90*	**3.02** *1.16*	**2.99** *1.25*
M11	**2.78** *1.39*	**2.80** *1.45*	**2.78** *1.09*	**3.10** *0.98*	**3.09** *1.14*	**3.09** *0.95*	**3.05** *1.16*	**3.02** *1.23*
ωB97X-D	**2.75** *1.39*	**2.78** *1.48*	**2.75** *1.10*	**3.05** *0.99*	**3.01** *1.08*	**3.01** *0.91*	**3.05** *1.17*	**3.01** *1.24*

Table 1 Vertical excitation energies (eV) of our prodigiosin model and obtatoclax in the neutral, protonated, and sodiated states using various functionals (6-311++G(d,p) basis set). Oscillator strengths are given in italics. For details on the nomenclature of the tautomers and rotamers, please see Text and Figures **??** and **??** in ESI. For each conformation, the geometry is fixed as obtained using ωB97X-D/6-311++G(d,p) optimization, and the relative energy (+ZPC) is given in parenthesis (kJ.mol^{-1}). At 300K, $k_BT \simeq 2.5$ kJ.mol^{-1}, some isomers are chosen not because of their low energy, but because they permit to discuss the impact of protonation and sodiation on the excitation energies (see Text).

D/6-311++G(d,p)). Such small differences between the rotamers of the neutral or protonated family might not be deciphered in the action mass spectra, but the family of neutral and protonated prodigiosin have energies different enough to be distinguished. There is one exception to this tendency: The difference of the vertical excitation energies of the neutral Iδ-PG and the protonated state Iδ-PG-H$^+$ is only 0.08 eV using ωB97X-D. But this result is functional dependent. The different in excitation energies becomes as large as 0.32 eV using the M11 functional. This rotamer could instructively be further studied using quantum chemistry methods preciser than TDDFT.

Looking in more detail at the dependance of the vertical excitation energies on the functional, the excitations energies vary from 2.53 to 2.83 eV for τ-HCTH and ωB97X-D respectively. These values are clearly above the energy deduced from the maximum of the photofragmentation spectrum (2.37 eV) by 0.16 eV to 0.46 eV. This difference had already been noticed by Tossel et al. who had used the B3LYP functional[52]. Such errors are typical of the TDDFT methods[54], but one could have hoped for a better accuracy from Global Hybrids functionals incorporating a large share of exact exchange (M11), or range-separated hybrids (e.g., CAM-B3LYP and ωB97X-D).

One origin of the shift of an absorption band relative to the prediction by vertical electronic energy can be the coupling between the electronic and vibrational excitations. The broadness and shift of the absorption band emerge from the electronic excitations from or towards vibrationally excited states. Vibronic couplings modify the absorption spectrum when the electronically excited state has a different geometry from the ground state. We have estimated the impact of this effect by calculating the form of the absorption band emerging from vibronic coupling for prodigiosin in neutral and protonated forms. Our calculations, based on the Franck-Condon formalism, are performed for molecules at 0K, i.e. it takes into account transitions from the ground state in its vibrationally ground state (initial quantum numbers $v = 0$) towards the electronic excited state in vibrationally excited states (final quantum numbers $v' \geq 0$). The adiabatic excitation energies (0-0 transitions) are 0.32 and 0.16 eV below the vertical excitation energies for Iβ-PG and IVγ-PG-H$^+$ respectively. Vibronic coupling is thus non negligible, but it is not anomalously high for an organic dye.

The vibronic coupling calculations provide thousands of absorption frequencies and associated intensities. To obtain a continuous spectrum comparable to experimental data, these absorption peaks have been convoluted with Gaussian functions, which width is adapted to match the broadening of the experimental spectra. This convolution mimics broadening due to Doppler effect and temperature. Fig. 3 compares the calculated absorption spectra of protonated prodigiosin IVγ-PG-H$^+$ and neutral prodigiosin Iβ-PG. These spectra are also overlaid with the experimental action spectra of Figs. 2a and 2b in ESI (Fig. **??**). The relative shape, position and intensities of the peaks of both the theoretical and experimental data match grossly, except for the tails of the absorption peaks, which are broader in the theoretical model. Indeed, the impact

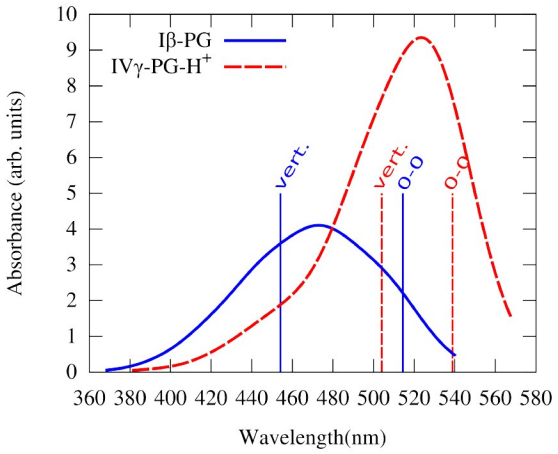

Fig. 3 Vibrationnally resolved absorption spectra of Iβ-PG and IVγ-PG-H$^+$ predicted by TDDFT calculations. The vertical lines show the position of an absorption peak deduced from the vertical transition energy (vert.) or from the adiabatic transition (0-0) . The energies calculated by TD-ωB97X-D/6-311++G(d,p) have all been shifted by -0.37 eV to match the peak position of the experimental data. The theoretical absorption energies have been convoluted with a Gaussian function with a half width at half maximum (HWHM) of about 0.1 eV. Color online.

of vibronic coupling is stronger for the neutral prodigiosin than for the protonated one, its calculated absorption band is broader and its intensity is lower. But within our approximations, vibronic coupling alone is not sufficient to explain the differences between the experimental and TD-ωB97X-D/6-311++G(d,p) absorption energies. To match the experimental and theoretical maxima of the peaks obtained using ωB97X-D/TDDFT and action spectroscopy, one needs to shift the theoretical energies by about -0.37 eV.

Despite the typical inaccuracy in the excitation energy, the TDDFT calculations are informative : The enlargements of the absorption band in the experimental action mass (Figs. 2a and 2b) are compatible with our calculated vibronic coupling. Moreover, the calculations also permit to determinate which vibrational modes contribute to the specific band shape of the system: For IVγ-PG-H$^+$, the first, second and 8th modes (starting from the lowest energy) are particularly important and are excited together. Mode 1 corresponds to a deformation of the molecule relative to its planar shape, cycle A and C flapping symmetrically like the wings of a flying butterfly. Mode 2

corresponds to the rotation of cycle A around bound (1) (see Fig. 1). Mode 8 corresponds to an in-plane rotations of cycles A and C. For Iβ-PG, 3rd and 4th modes are particularly important. They both correspond to the opening of the tweezer formed by the three nitrogen atoms, with an approximate conservation of the planarity of the molecule.

To summarize, from these first results on our prodigiosin model, one could expect that experimental absorption spectra or action spectra of prodigiosin could permit to distinguish between different protonation states, but not between rotamers. The origin of the width of the peak on the action spectra of PG and PG-H^+ seems to be the coupling between electronic and vibrational excitations, rather than the presence of several isomers or several electronic excitations.

3.3.2.2 Protonated and neutral obatoclax

The conclusions made on PG theoretical results hold also for OBX too : the absorption wavelength and absorption intensities decrease upon deprotonation. Again, this is in qualitative agreement with what is observed for the absorption spectra of obatoclax in solutions. Again, the vertical excitation energies are mostly of few tenths of eV above the energies obtained from the action mass spectra.

Concerning the theoretical predictions, the results depend on the functionals: the τ-HCTH, B3LYP and PBE0 functionals predict two electronic excitations for IVγ-OBX-H^+. The former one, τ-HCTH, even predicts two peaks of similar intensities at 2.25 and 2.46 eV, which are very close to two peaks observed on the action spectra at 2.23 and 2.39 eV. Other functionals, among which our choice ωB97X-D, and also the praised M11 and CAM-B3LYP, predict a single electronic excitation at 2.75, 2.78 and 2.80 eV respectively. Moreover, τ-HCTH, B3LYP and PBE0 functionals predict significant differences between the two rotamers IVγ-OBX-H^+ and IVα-OBX-H^+, while M11 and CAM-B3LYP predict very similar electronic excitations.

Due of this difficulty for the TDDFT results to draw clear conclusions on the vertical electronic excitations of obatoclax, we did not investigate further towards the shape of its absorption bands. Unfortunately, we cannot clearly attribute the double peak appearing in the action-spectrum of the OBX-H^+ to either a single electronic excitation with some vibronic coupling, or two separated electronic excitations. The presence of two rotamers also remains a possibility to explain the presence of the two peaks, but in this case, the distribution of the two rotamers in the ion trap is far from the equilibrium Boltzmann distribution given by the relative total energies. To clarify these points, it would be helpful to study theoretically the electronic excitations of protonated obatoclax using post-Hartree-Fock approaches with higher accuracy than TDDFT.

3.3.3 Interactions with Na^+ As our aim is to investigate prodigiosin and obatoclax in complex environments, the impact of electrostatic interactions on their structure and absorption spectra should be further investigated. Here, we focus on the impact of the complexation with a sodium cation.

The geometries of the complexes of the neutral PG and OBX with sodium cation were optimized. To guess reasonable initial structures, the electrostatic potentials of the optimized neutral species were studied. As expected, the electronegative regions are located (1) in the vicinity of the nitrogen which does not carry any proton, (2) on both sides of the three cycles A, B and C, and (3) on the two lone pairs of the methoxy group. Following these hints, we constructed 10 starting positions for the sodium cation dispatched on these electronegative regions for each of the 24 neutral isomers, and optimized their geometries. Fig. 4 illustrates the structure of optimized conformers of PG-Na^+ and OBX-Na^+. First, the case of prodigiosin is discussed. The PG-Na^+ with the lowest calculated energy among all calculations is of type Iζ-PG-Na^+ (Fig. 4a). For comparison the one with the lowest energy among the Iβ-PG-Na^+ type lies 12 kJ.mol^{-1} higher in energy. This latter one would be obtained by adding a sodium cation to the most stable conformer of neutral PG (Iβ), if the exchange between rotamers would be frozen, which may happen in a confined or viscous environment, like in a protein or in a lipidic membrane. All the low-energy conformations of PG-Na^+ are favored by both a strong electrostatic interaction between the bare nitrogen and the Na^+, but also by π-cation interactions with cycle C. A compromise has to be found between maximizing interaction with the cation and maximizing the planarity of the aromatic moiety. Because of their bulkiness, the substituents of cycle C also have an impact on the stability of the different isomers. The dihedral angle around bound (3) of Fig. 1 is about 30 degrees in the most stable conformer Iζ-PG-Na^+, and as large as 50 degrees in the less stable Iβ-PG-Na^+. Noticeably, the presence of the sodium cation favors conformations of PG-Na^+ like Iζ, Iε and Iδ, which are improbable in its absence. These lie respectively at energies 3.9, 6.2 and 6.7 kJ.mol^{-1} higher than the most stable state Iζ-PG-Na^+, and could therefore be present in small amount at equilibrium.

The rotamers favored in sodiated obatoclax are rather different for the ones in sodiated prodigiosin. As for PG-Na^+, the sodium cation interacts with both the bare nitrogen and the delocalized π electrons (see Figs. 4, c and d) but whereas it interacts with cycle C in PG-Na^+, in OBX-Na^+ it interacts with cycle A. The hydrogen bond between the methoxy group and the nitrogen of cycle C remains present in the Iγ-OBX-Na^+ and Iα-OBX-Na^+. It turns out that the most favorable conformers are the same for OBX-H^+ and OBX-Na^+, but this seems fortuitous. Again, a compromise has to be found between maximizing interaction with the cation and maximizing the planarity of the aromatic moiety. The dihedral angle around bound (1) of is about 42 degrees in the most stable conformer Iγ-OBX-Na^+ (see Fig. 4c).

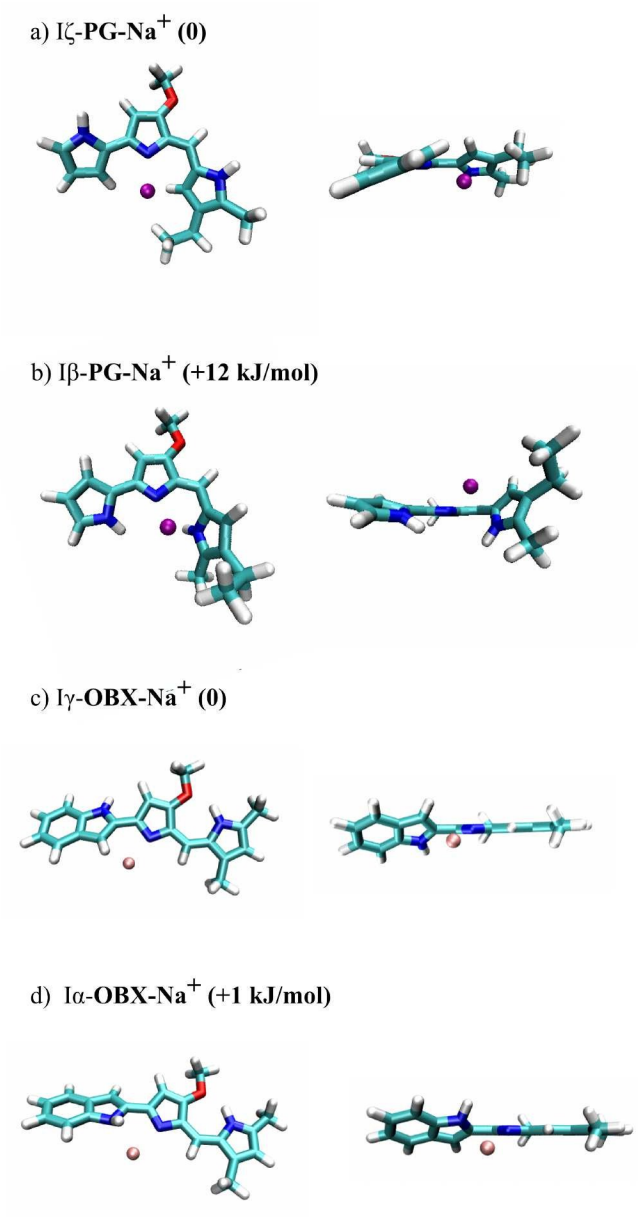

Fig. 4 Optimized structures of sodiated prodigiosin (a,b) and sodiated obatoclax (c,d). The sodium cation is represented as a pink sphere. Only some optimized conformers are selected here. The relative total energy is given in parenthesis. (a) Iζ-PG-Na$^+$ has the lowest calculated energy among all calculations of PG-Na$^+$. (b) The complex with the lowest energy among the Iβ-PG-Na$^+$. (c) Iγ-OBX-Na$^+$ has the lowest calculated energy among all calculations of OBX-Na$^+$. (d) Iα-OBX-Na$^+$ is just 1 kJ.mol^{-1} higher in energy. Color online.

Especially for conjugated moieties, such perturbations of the molecular geometry may strongly influence the electronic structure and electronic excitations[70]. Table 1 gathers the vertical absorption energies obtained for sodiated prodigiosin and obatoclax. Depending on the isomers, the interaction with sodium cation has different impacts. For the most stable isomer Iζ-PG-Na$^+$, for example, the presence of a sodium ion has practically no impact on the geometry of prodigiosin and on the absorption energy. In contrast, for the Iβ-PG isomer, the interaction with the cation distorts the planar structure of the conjugated moiety. This decreases the electronic delocalization, therefore increases the gap between the highest occupied molecular orbital (HOMO) and lowest unoccupied molecular orbital (LUMO). The distortion by Na$^+$ destabilizes so strongly the Iβ-PG, that this isomer would no longer be relevant in an equilibrated sample in a complex with Na$^+$. If one compares the vertical excitation energies of Iβ-PG and Iβ-PG-Na$^+$ (see Table 1), this effect appears functional dependent, with the largest effect for functional taking into account dispersion effects and containing exact-exchange contributions. But if one compares the two lowest-energy states before and after sodiation : Iβ-PG and Iζ-PG-Na$^+$, the vertical excitation energies are almost the same. We attribute this similarity to the conformers favored during the interaction with the sodium with only small deformations. Similarly, for OBX, if one compares the two lowest-energy states before and after sodiation: Iβ-OBX and Iγ-OBX-Na$^+$, the vertical excitation energies are practically the same.

4 Conclusions

In summary, we have studied the optical properties of prodigiosin and obatoclax by using action spectroscopy and theoretical calculations. They exist as free bases or protonated species and both can interact with cations or anions.

The action spectroscopy of the protonated and sodiated species shows that the spectra of the ionic species are different enough to be clearly distinguished. We investigated the impact of solvent and of complexation with sodium on the absorption energies. The solvatochromic effect is practically negligible.

Density Functional Theory (DFT) and Time-Dependent DFT (TDDFT) results permit to interpret the action spectra in term of electronic excitation with strong vibronic coupling. The interconversion between isomers can clearly be dragged by the environment, either a change of pH, or by the presence of ions. The excitation energies depend the molecule's protonation state, but much less on the dielectric constant of the solvent, possible isomerization, or the presence of a sodium cation.

These prodiginins optical properties may open the door for new experimental investigations of this important family of ligand in biomimetic environment.

*Acknowledgements*A.-R. Allouche is acknowledged for motivating discussions. Pôle Scientifique de Modélisation Numérique from the ENS Lyon (PSMN), Centre Informatique National de l'Enseignement Supérieur (CINES, Montpelier, France) and Institut du Développement et des Ressources en Informatique Scientifique (IDRIS) are acknowledged for computing time allocation (Project c2014085142).

*Electronic Supplementary Information*Absorption Spectra of prodigiosin and obatoclax in solution under various pH. Plots of absorption maxima in various solvents vs the dielectric constant for prodigiosin and obatoclax. Electrospray CID-MS2 spectra for protonated and sodiated prodigiosin. Calculated total energies for the 32 conformers of our model prodigiosin and obatoclax, neutral and protonated forms. Comparison of the gas-phase action spectra of protonated and sodiated prodigiosin, with the calculated absorption spectra of protonated and neutral prodigiosin.

References

1 J. A. Green, D. A. Rappoport and R. P. Williams, *J. Bacteriol.*, 1956, **72**, 483–487.
2 J. Y. D'Aoust and N. N. Gerber, *J. Bacteriol.*, 1974, **118**, 756–757.
3 G. Hobbs, C. M. Frazer, D. C. J. Gardner, F. Flett and S. G. Oliver, *J Gen Microbiol*, 1990, **136**, 2291–2296.
4 R. D'Alessio, Alberto Bargiotti, Orlando Carlini, Francesco Colotta, Mario Ferrari, Paola Gnocchi, Annamaria Isetta, Nicola Mongelli, Pietro Motta, Arsenia Rossi, M. and Marcello Tibolla and Vanotti, Ermes, *J. Med. Chem.*, 2000, **43**, 2557–2565.
5 T. Kawasaki, F. Sakurai and Y. Hayakawa, *J. Nat. Prod.*, 2008, **71**, 1265–1267.
6 N. Staric, T. Danevcic and D. Stopar, *Microbial Ecology*, 2010, **60**, 592–598.
7 A. Fürstner, *Ang. Chem. In. Ed.*, 2003, **42**, 3582–3603.
8 N. Stankovic, L. Senerovic, T. Ilic-Tomic, B. Vasiljevic and J. Nikodinovic-Runic, *Applied Microbiol. Biotechnol.*, 2014, **98**, 3841–3858.
9 M. Nguyen, R. C. Marcellus, A. Roulston, M. Watson, L. Serfass, S. R. Murthy Madiraju, D. Goulet, J. Viallet, L. Bélec, X. Billot, S. Acoca, E. Purisima, A. Wiegmans, L. Cluse, R. W. Johnstone, P. Beauparlant and G. C. Shore, *Proc. Nat. Ac. Sci.*, 2007, **104**, 19512–19517.
10 C. A. Goard and A. Schimmer, *Core Evidence*, 2013, 15–26.
11 S. Trudel, Z. H. Li, J. Rauw, R. E. Tiedemann, X. Y. Wen and A. K. Stewart, *Blood*, 2007, **109**, 5430–5438.
12 M. Konopleva, J. Watt, R. Contractor, T. Tsao, D. Harris, Z. Estrov, W. Bornmann, H. Kantarjian, J. Viallet, I. Samudio and M. Andreeff, *Cancer Res.*, 2008, **68**, 3413–3420.
13 C. Campàs, A. M. Cosialls, M. Barragán, D. Iglesias-Serret, A. F. Santidrián, L. Coll-Mulet, M. de Frias, A. Domingo, G. Pons and J. Gil, *Exp. Hematol.*, 2006, **34**, 1663–1669.
14 P. Pérez-Galán, G. Roué, N. Villamor, E. Campo and D. Colomer, *Blood*, 2007, **109**, 4441–4449.
15 C. Mitchell, A. Yacoub, H. Hossein, A. P. Martin, M. D. Bareford, P. Eulitt, C. Yang, K. P. Nephew and P. Dent, *Cancer Biol. Ther.*, 2010, **10**, 903–917.
16 S. Huang, K. Okumura and F. A. Sinicrope, *Clin. Cancer Res.*, 2009, **15**, 150–159.
17 T. Sato, H. Konno, Y. Tanaka, T. Kataoka, K. Nagai, H. H. Wasserman and S. Ohkuma, *J. Biol. Chem.*, 1998, **273**, 21455–21462.
18 S. Ohkuma, T. Sato, M. Okamoto, H. Matsuya, K. Arai, T. Kataoka, K. Nagai and H. H. Wasserman, *Biochem. J.*, 1998, **334 (Pt 3)**, 731–741.
19 J. L. Sessler, L. R. Eller, W. S. Cho, S. Nicolaou, A. Aguilar, J. T. Lee, V. M. Lynch and D. J. Magda, *Ang. Chem. Int. Ed.*, 2005, **44**, 5989–5992.
20 S.-K. Ko, S. K. Kim, A. Share, V. M. Lynch, J. Park, W. Namkung, W. Van Rossom, N. Busschaert, P. A. Gale, J. L. Sessler and I. Shin, *Nature Chemistry*, 2014, **6**, 885–892.
21 G. Park, J. T. Tomlinson, M. S. Melvin, M. W. Wright, C. S. Day and R. A. Manderville, *Organic Letters*, 2003, **5**, 113–116.
22 A. Fürstner and E. J. Grabowski, *Chembiochem*, 2001, **2**, 706–709.
23 C. L. Z. N.-C. Naval Bajwa, *Expert Op. Ther. Pat.*, 2012, **22**, 37–55.
24 L. Han, Y. Zhou, X. Huang, M. Xiao, L. Zhou, J. Zhou, A. Wang and J. Shen, *Spectrochim. Acta A: Molecular and Biomolecular Spectroscopy*, 2014, **123**, 497–502.
25 P. A. Gale, R. Pérez-Tomás and R. Quesada, *Accounts Chem. Res.*, 2013, **46**, 2801–2813.
26 Y. Harazono, K. Nakajima and A. Raz, *Cancer Metastasis Rev*, 2014, **33**, 285–294.
27 M. S. Melvin, J. T. Tomlinson, G. Park, C. S. Day, G. R. Saluta, G. L. Kucera and R. A. Manderville, *Chem. Res. Toxicol.*, 2002, **15**, 734–741.
28 S. Jenkins, C. D. Incarvito, J. Parr and H. H. Wasserman, *CrystEngComm*, 2009, **11**, 242–245.
29 M. García-Valverde, I. Alfonso, D. Quiñonero and R. Quesada, *J. Org. Chem.*, 2012, **77**, 6538–6544.
30 V. Rizzo, A. Morelli, V. Pinciroli, D. Sciangula and R. D'Alessio, *J. Pharm. Sci.*, 1999, **88**, 73–78.
31 A. V. Onufriev and E. Alexov, *Quarterly Rev. Biophys.*, 2013, **46**, 181–209.
32 N. Shimba, Z. Serber, R. Ledwidge, S. M. Miller, C. S. Craik and V. Dötsch, *Biochem.*, 2003, **42**, 9227–9234.
33 Hudáky, Péter and Perczel, András, *J. Comput. Chem.*, 2005, **26**, 1307–1317.
34 Waszkowycz, Bohdan, Clark, David E and Gancia, Emanuela, *WIREs Comput. Mol. Sci.*, 2011, **1**, 229–259.
35 E. Yuriev and P. A. Ramsland, . *Mol. Recognit.*, 2013, **26**, 215–239.
36 R. Antoine and P. Dugourd, *Phys. Chem. Chem. Phys.*, 2011, **13**, 16494–16509.
37 S. B. Nielsen, A. Lapierre, J. U. Andersen, U. V. Pedersen, S. Tomita and L. H. Andersen, *Phys. Rev. Lett.*, 2001, **87**, 228102.
38 K. Chingin, R. M. Balabin, V. Frankevich, K. Barylyuk, R. Nieckarz, P. Sagulenko and R. Zenobi, *Int. J. Mass Spect.*, 2011, **306**, 241–245.
39 M. D. Davari, F. J. A. Ferrer, D. Morozov, F. Santoro and G. Groenhof, *ChemPhysChem*, 2014, **15**, 3236–3245.
40 M. W. Forbes, A. M. Nagy and R. A. Jockusch, *Inter. J. Mass Spect.*, 2011, **308**, 155–166.
41 M. Wanko, J. Houmoller, K. Stochkel, M.-B. S. Kirketerp, M. A. Petersen, M. B. Nielsen, S. B. Nielsen and A. Rubio, *Phys. Chem. Chem. Phys.*, 2012, **14**, 12905–12911.
42 B. B. Kirk, A. J. Trevitt, S. J. Blanksby, Y. Tao, B. N. Moore and R. R. Julian, *The Journal of Physical Chemistry A*, 2013, **117**, 1228–1232.
43 K. Matheis, L. Joly, R. Antoine, F. Lepine, C. Bordas, O. T. Ehrler, A.-R. Allouche, M. M. Kappes and P. Dugourd, *J. Am. Chem. Soc.*, 2008, **130**, 15903–15906.
44 L. Joly, R. Antoine, A.-R. Allouche, M. Broyer, J. Lemoine and P. Dugourd, *J. Am. Chem. Soc.*, 2007, **129**, 8428–8429.
45 C. Brunet, R. Antoine, J. Lemoine and P. Dugourd, *J. Phys. Chem. Lett.*, 2012, **3**, 698–702.
46 Bellina, Compagnon, Joly, Albrieux, Allouche, Bertorelle, Lemoine and Antoine, *Int. J. Mass. Spectrom.*, 2010, **297**, 5–5.
47 C. Brunet, R. Antoine, P. Dugourd, F. Canon, A. Giuliani and L. Nahon,

J. Chem. Phys., 2013, **138**, 064301.

48 C. Brunet, R. Antoine, A.-R. Allouche, P. Dugourd, F. Canon, A. Giuliani and L. Nahon, *J. Phys. Chem. A*, 2011, **115**, 8933–8939.

49 D. P. Dimitrov, *Zeitschrift für Naturforschung B*, 1970, **25**, 762–763.

50 L. Han, Y. Zhou, X. Huang, M. Xiao, L. Zhou, J. Zhou, A. Wang and J. Shen, *Spectrochimica Acta Part A: Molecular and Biomolecular Spectroscopy*, 2014, **123**, 497–502.

51 B. Bellina, R. Antoine, M. Broyer, L. Gell, Ž. Sanader, R. Mitrić, V. Bonačić-Koutecký and P. Dugourd, *Dalton Trans.*, 2013, **42**, 8328–8333.

52 J. A. Tossell, *Compt. Theor. Chem.*, 2012, **997**, 103–109.

53 M. J. Frisch, G. W. Trucks, H. B. Schlegel, G. E. Scuseria, M. A. Robb, J. R. Cheeseman, G. Scalmani, V. Barone, B. Mennucci, G. A. Petersson, H. Nakatsuji, M. Caricato, X. Li, H. P. Hratchian, A. F. Izmaylov, J. Bloino, G. Zheng, J. L. Sonnenberg, M. Hada, M. Ehara, K. Toyota, R. Fukuda, J. Hasegawa, M. Ishida, T. Nakajima, Y. Honda, O. Kitao, H. Nakai, T. Vreven, J. A. Montgomery, Jr., J. E. Peralta, F. Ogliaro, M. Bearpark, J. J. Heyd, E. Brothers, K. N. Kudin, V. N. Staroverov, R. Kobayashi, J. Normand, K. Raghavachari, A. Rendell, J. C. Burant, S. S. Iyengar, J. Tomasi, M. Cossi, N. Rega, J. M. Millam, M. Klene, J. E. Knox, J. B. Cross, V. Bakken, C. Adamo, J. Jaramillo, R. Gomperts, R. E. Stratmann, O. Yazyev, A. J. Austin, R. Cammi, C. Pomelli, J. W. Ochterski, R. L. Martin, K. Morokuma, V. G. Zakrzewski, G. A. Voth, P. Salvador, J. J. Dannenberg, S. Dapprich, A. D. Daniels, . Farkas, J. B. Foresman, J. V. Ortiz, J. Cioslowski and D. J. Fox, *Gaussian09 Revision D.01*, Gaussian Inc. Wallingford CT 2009.

54 A. D. Laurent and D. Jacquemin, *Int. J. Quant. Chem.*, 2013, **113**, 2019–2039.

55 D. Jacquemin, V. Wathelet, E. A. Perpète and C. Adamo, *J. Chem. Theory Comput.*, 2009, **5**, 2420–2435.

56 J. Preat, D. Jacquemin and E. A. Perp e te, *Int. J. Quantum Chem.*, 2010, **110**, 2147–2154.

57 D. Jacquemin, B. Mennucci and C. Adamo, *Phys. Chem. Chem. Phys.*, 2011, **13**, 16987–16998.

58 J.-D. Chai and M. Head-Gordon, *Phys Chem Chem Phys*, 2008, **10**, 6615–6620.

59 Jacquemin, Denis, Perpète, Eric A, Ciofini, Ilaria and Adamo, Carlo, *Theor. Chem. Acc.*, 2011, **128**, 127–136.

60 A. D. Becke, *J. Chem. Phys.*, 1993, **98**, 5648–5652.

61 Boese, A D and Handy, N C, *J. Chem. Phys.*, 2002, **116**, 9559–9569.

62 Yanai, T., *Chem. Phys. Lett.*, 2004, **393**, 51–57.

63 C. Adamo and V. Barone, *J. Chem. Phys.*, 1999.

64 R. Peverati and D. G. Truhlar, *Philos Trans A Math Phys Eng Sci*, 2014, **372**, 20120476.

65 Y. Zhao and D. G. Truhlar, *Acc. Chem. Res.*, 2008, **41**, 157–167.

66 F. Santoro, A. Lami, R. Improta and V. Barone, *J. Chem. Phys.*, 2007, **126**, 184102.

67 Santoro, Fabrizio, Lami, Alessandro, Improta, Roberto, Bloino, Julien and Barone, Vincenzo, *J. Chem. Phys.*, 2008, **128**, 224311.

68 W. R. Hearn, J. Medina-Castro and M. K. Elson, *Nature*, 1968, **220**, 170–171.

69 K. Chen, N. Rannulu, Y. Cai, P. Lane, A. Liebl, B. Rees, C. Corre, G. Challis and R. Colewasz, *J. Am. Soc. Mass Spect.*, 2008, **19**, 1856–1866.

70 C. Loison, R. Antoine, M. Broyer, P. Dugourd, J. Guthmuller and D. Simon, *Chem. Eur. J.*, 2008, **14**, 7351–7357.